Journal of Engineering and Technology Vol.5, No.2, 2006 ISSN 1684-4114

Numerical simulation of the effect of turbulence strength on shock/turbulence interaction

Mohammad Ali Jinnah*, Kazuyoshi Takayama**

Abstract

Shock wave interactions with different strengths of turbulence are observed numerically by solving the time-dependent three-dimensional Navier-Stokes equations with k-ε turbulence model for a compressible fluid. Numerical measurements are taken before and after the interaction of the reflected shock wave with different turbulent regions located along the longitudinal distance behind the turbulence-generating grids in the shock tube. All turbulent fluctuations are measured for the shock wave interaction with the turbulence of different strengths and it is observed that the longitudinal turbulence intensity and turbulent kinetic energy level are amplified and the amplification is higher in interaction of shock wave with comparatively weak turbulence. Due to stronger compressibility effects on the turbulent field, all length scales are decreased more after the shock/turbulence interaction. After the shock/turbulence interaction, the dissipation rate of turbulent kinetic energy decreases in all the cases of the strength of turbulent fields and the decreasing of the dissipation rate is higher for the stronger turbulence field.

Keywords : Shock wave, Turbulent flow, Navier-Stokes equations, Turbulence model, Shock /turbulence interaction

1 Introduction

The investigations on the effect of turbulence strength on shock/turbulence interaction are conducted in this paper and it is one of the innovative works on shock/turbulence interaction. After computing the turbulence fluctuations, a numerical simulation by

* MCE Department, Islamic University of Technology, Board Bazar, Gazipur-1704

** Multidisciplinary Shock Wave Research Center, Tohoku University, 2-1-1 katahira, Aoba-ku, Sendai 980-8577, Japan

Jinnah and Takayama [1], was carried out at different strengths of shock wave and it is concluded that the amplification of turbulence fluctuations is lower in strong shock/turbulence interaction. The amplification of longitudinal turbulence fluctuations and turbulent kinetic energy level after interaction depend on the strength of turbulence. To generate a turbulent field behind the shock wave, turbulence-generating grids are placed in the shock tube. The shock wave after passing through the turbulence-generating grids generates a turbulence field where near the grid plate, the turbulent field will be stronger and the turbulent field strength will decrease at the far distance from the grid plate. Due to turbulence decay along the centerline of the shock tube, the strengths of turbulence at different points on the centerline of the shock tube are different. So in the present computations, the turbulent fields of different strengths are selected along the centerline of the shock tube. The reflected shock wave after reflection from the end wall interacts with different turbulent fields and the outcomes of shock/turbulence interaction in different turbulent fields are observed numerically. The turbulence length scales also vary in interaction of shock wave with different strengths of turbulent fields and the turbulence length scales are decreased more in interaction of shock wave with comparatively stronger turbulent field. In shock/turbulence interaction, the rate of dissipation of turbulent kinetic energy decreases in all the cases of strength of turbulent fields and the higher dissipation is found in interaction of shock wave with strong turbulence. Experimental realization of a homogeneous and isotropic turbulent flow interacting with a normal shock wave in the laboratory is a difficult task due to generation of compressible and isotropic turbulent flow and the generation of a normal shock wave interacting with flow. Experimentally and numerically many researchers got many results on shock/turbulence interaction. The outcomes of the interactions of shock wave with homogeneous and isotropic turbulence are the amplification of longitudinal velocity fluctuations, the amplification of turbulent kinetic energy level and substantial changes in length scales. Debreve and Lacharme [2] conducted experiments on the interaction between the shock wave and grid-generated turbulence and they measured velocity and temperature spectra upstream and downstream of the shock wave and concluded that turbulent fluctuations are amplified and Taylor micro scales increase during the interaction. Jacquin, Blin and Gaffray [3] investigated the interactions of a normal shock wave with grid-generated turbulence and a turbulent jet and they observed that turbulence amplification was not significant for the grid-generated

turbulence and that the decay of turbulent kinetic energy was accelerated downstream of the shock wave. Their experiments treated the interaction of a shock with quasi-incompressible turbulence where fluctuations in pressure and density are not significant. An experiment on the interaction of weak shocks (M_s = 1.007, 1.03 and 1.1) with a random medium of density in homogeneity was performed by Hesselink and Sturtevant [4]. They observed that the pressure histories of the distorted shock waves were both peaked and rounded and explained these features in terms of the focusing/defocusing of the shock front due to in homogeneity of the medium. Numerical techniques for such types of interactions are more suitable to get the reliable results and easily estimate the physical data structure, which can difficult to measure in experiment. Using a shock capturing numerical technique, Rotman [5] numerically calculated the change in a two-dimensional turbulent flow caused by the passage of a traveling shock wave. He found that the shock causes in increase in the turbulent kinetic energy and that the length scale of the turbulent field is reduced upon passage of the shock. He also found that increasing the initial turbulent kinetic energy caused a straight shock wave to evolve into a distorted front. Lee, Lele and Moin [6] conducted direct numerical simulations of two-dimensional turbulence interacting with a shock wave and found that vorticity amplification compared well with the predictions of the linear analysis but turbulent kinetic energy evolution behind the shock showed significant nonlinear effects. For the present numerical simulation, the three-dimensional Navier-stokes equations using k-ε turbulence model, are solved by shock capturing method where for more accurate solutions, the grid adaptation technique is used. Grid adaptation technique with k-ε turbulence model are the improve technique for numerical simulation of shock/turbulence interaction.

2 Numerical Methods

2.1 Governing equations

For the present computations, the three-dimensional numerical code is used to find out the effect of turbulence strength on shock/turbulence interaction. By using the same numerical code, the computational results, computed by Jinnah and Takayama [7], was used to find out the effect of longitudinal velocity across the shock on shock/turbulence interaction. Without external forces and heat sources, the conservative form of non-dimensionalized

governing equation in three-dimensional Cartesian coordinate system is

$$\frac{\partial Q}{\partial t}+\frac{\partial (F-Fv)}{\partial x}+\frac{\partial (G-Gv)}{\partial y}+\frac{\partial (H-Hv)}{\partial z}=S(Q)$$

where $Q = [\rho, \rho u, \rho v, \rho w, e, \rho k, \rho \varepsilon]$, the vector of conservative variables which contains mass, momentum and energy. All variables are calculated in per unit volume. ρ is taken as the mass per unit volume. Three momentum terms in three-dimensional Cartesian coordinates system are ρu, ρv and ρw per unit volume. Total energy, e, turbulent kinetic energy, ρk and turbulent dissipative energy, $\rho \varepsilon$ are the energy terms per unit volume in these computations. F, G and H are the three inviscid flux vectors in X-, Y-, and Z-axis respectively. Similarly F_v, G_v and H_v are the three viscous flux vectors in X-, Y-, and Z-axis respectively. Also ρ is the fluid density and u, v and w are velocity components in each direction of Cartesian coordinates. While e is the total energy per unit volume, pressure p can expressed by the following state equation for ideal gas

$p = (\gamma -1)[e -\frac{1}{2} \rho(u^2+ v^2+ w^2)]$ where γ is the ratio of specific heats.

The source term $S(Q)$ of the k-ε turbulence model is written by

$S(Q)= [\, 0, 0, 0, 0, 0, P_k -\rho\varepsilon - D_k, (c_{\varepsilon 1} P_k - c_{\varepsilon 2} \rho\varepsilon)\frac{\varepsilon}{k}\,]$

where the production term P_k is given in Cartesian coordinates as

$$P_k = \{ 2\mu_t \frac{\partial u}{\partial x} -\frac{2}{3} [\rho k+ \mu_t(\frac{\partial u}{\partial x} +\frac{\partial v}{\partial y} +\frac{\partial w}{\partial z})]\} \frac{\partial u}{\partial x} +\{ 2\mu_t \frac{\partial v}{\partial y} -\frac{2}{3} [\rho k+ \mu_t(\frac{\partial u}{\partial x} +\frac{\partial v}{\partial y} +\frac{\partial w}{\partial z})]\} \frac{\partial v}{\partial y} +$$

$$\{ 2\mu_t \frac{\partial w}{\partial z} -\frac{2}{3} [\rho k+ \mu_t(\frac{\partial u}{\partial x} +\frac{\partial v}{\partial y} +\frac{\partial w}{\partial z})]\} \frac{\partial w}{\partial z} + \mu_t(\frac{\partial u}{\partial y} +\frac{\partial v}{\partial x})^2+$$

$$\mu_t(\frac{\partial u}{\partial z} +\frac{\partial w}{\partial x})^2+ \mu_t(\frac{\partial w}{\partial y} +\frac{\partial v}{\partial z})^2$$

and the destruction term D_k is given as $D_k = \frac{2\rho}{\gamma T} k\varepsilon$

The mass average turbulent kinetic energy and homogeneous component of turbulent kinetic energy dissipation rate are defined by as $k = \frac{1}{2}\ c_t^2\ (u^2+v^2+w^2)$ and $\varepsilon = c_m k^2 \frac{\mathrm{Re}}{100}$

The various constants in the k-ε turbulence model are listed as follows:
$c_\mu = 0.09$, $c_t = 0.03$, $c_m = 0.09$, $c_{\varepsilon 1} = 1.45$, $c_{\varepsilon 2} = 1.92$, $\sigma_k = 1.00$, $\sigma_\varepsilon = 1.30$

The governing equations described above for compressible viscous flow are discretised by the finite volume method. A second-order,

upwind Godunov scheme of Flux vector splitting method is used to discrete the inviscid flux terms and MUSCL-Hancock scheme with k-ε turbulence model is used for interpolation of variables where HLL Reimann solver is used for shock capturing in the flow. Central differencing scheme is used in discretizing the viscous flux terms. The upstream of incident shock wave is set as inflow boundary condition, the properties and velocities of which are calculated from Rankine-Hugoniot conditions with incident shock Mach number. The downstream inflow boundary condition and wall surface are used as solid boundary conditions where the gradients normal to the surface are taken zero. All solid walls are treated as viscous solid wall boundary. For the two-equation k-ε turbulence model on solid boundaries, μ_t is set to zero.

2.2 Grid Systems and Grid Adaptation

Three dimensional hexahedral cells with adaptive grids are used for these computations. In this grid system, the cell-edge data structures are arranged in such a way that each cell contains six faces which are sequence in one to six and each face indicates two neighboring cells that is left cell and right cell providing all faces of a cell are vectorized by the position and coordinate in the grid system. The initial three-dimensional grid system with turbulence-generating grids is shown in Fig.1. The physical size of each cell before adaptation is equal to 5x5x5 *(mm)* and the initial number of cell is 2876.

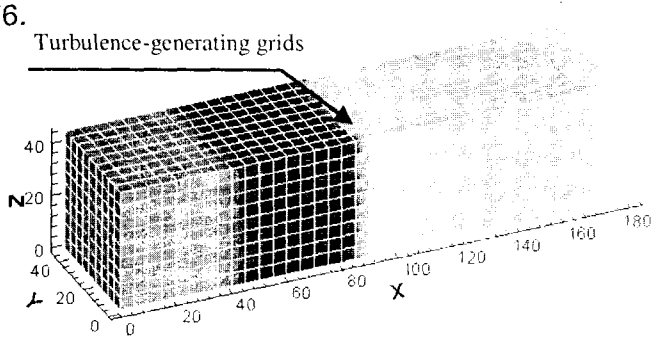

Fig.1: Three-dimensional grids and the position of the turbulence-generating grids

The grid adaptation is one of the improved and computational time saving techniques, which is used in these computations. The grid adaptation is performed by two procedures, one is refinement procedure and another is coarsening procedure. The refinement and coarsening operations are handled separately in computation.

The criterion used for grid adaptation is based on the truncation error (ϵ_T) of the Taylor series expansion of density. The truncation error indicator ϵ_T is defined for every face of a cell and given by the ratio of the second-order derivative term to the first order one of the Taylor series of density so that

$$\epsilon_T = max\left[\frac{|(\nabla\rho)_{lc} - (\nabla\rho)_i|}{(\alpha_f \rho_c)/dl + |(\nabla\rho)_i|}, \frac{|(\nabla\rho)_{lc} - (\nabla\rho)_j|}{(\alpha_f \rho_c)/dl + |(\nabla\rho)_j|}\right]$$

where c represent the location of any face of a cell and i and j represent left cell and right cell of that face, dl is the center distance between cell i and j, $(\nabla\rho)_i$ and $(\nabla\rho)_j$ are the density gradient for cell i and j, $(\nabla\rho)_{lc} = (\rho_i - \rho_j)/dl$, ρ_c is the density at the interface of right cell and left cell and α_f is the constant which is initially designed to prevent a zero denominator. The value of α_f is used 0.02 and it is problem-independent parameter. The refinement and coarsening operation for any cell depends on ϵ_T value and the value of ϵ_T is determined for each face of a cell. The criterion for adaptation for any cell is

Refinement=maximum ϵ_T of six faces of a cell $>\varepsilon_r$

Coarsening=maximum ϵ_T of six faces of a cell $<\varepsilon_c$

where ε_r and ε_c are the threshold values for refinement and coarsening. In these computations, the value of ε_r is used 0.44 and the value of ε_c is used 0.40 and the level of refinement is 2.

In the refinement procedure, the cells are selected for refinement in which every cell is divided into eight new sub cells and these new sub cells are arranged in a particular sequence so that these sub cells are used suitably in the data-structure. In the coarsening procedure, the eight sub cells, which are generated from the primary cell, are restored into the primary cell. The above three-dimensional adaptation strategy is an upgraded work of two-dimensional adaptation (Sun and Takayama [8]).

3 Results and Discussion

For the numerical simulation, turbulence-generating grids are placed in the shock tube parallel to *YZ*-plane and the position of turbulence-generating grids is shown in Fig.1. The total opening area of turbulence-generating grids is 50.6 % and the configuration of the turbulence-generating grids is shown in Fig.2.

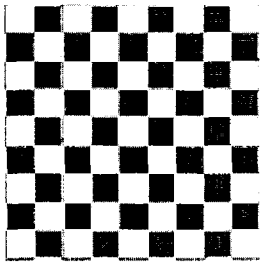

Fig.2: The configuration of the turbulence-generating grids

Turbulence-generating grids are uniform in size and spacing; so the shock wave and the gas flow following the shock wave after passing through turbulence-generating grids generate a compressible flow of homogeneous, isotropic turbulence. Three turbulent regions are selected behind the turbulence-generating grids with equal longitudinal distance. The region between lateral planes AA and BB is region-1, the region between lateral planes BB and CC is region-2 and the region between lateral planes CC and DD is region-3 which are shown in Fig.3.

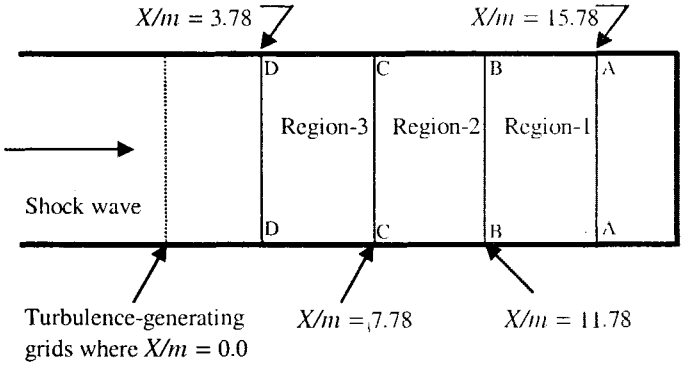

Fig.3: Sectional view of *ZX*-plane where the location of different turbulent regions

The centerline along the longitudinal direction of the turbulent regions is treated as the centerline of the turbulent regions. 11 points of equal spacing are taken on the centerline of each turbulent region and all turbulent parameters (velocity fluctuations, pressure fluctuations etc.) are computed on these 11 points for each turbulent region. The lateral planes intersect these points and parallel to the *YZ*-plane are treated as grid-data planes and the

grids inside the turbulent regions cut by the grid-data plane are the grids on the grid-data plane. The value of the turbulent parameter on the centerline of the turbulent regions is the average value of all the grid values of that parameter on the grid-data plane. All the relevant turbulent parameters are determined along the centerline of turbulent regions at the moment of reflected shock before entering into the turbulent region and after interaction the turbulent region. The selected three turbulent regions must exhibit with different strengths of turbulent field and in this paper; it is trying to clarify the interactions of normal shock with different strengths of turbulent field. The longitudinal distances (*X/m*) of any point on the centerline of turbulent regions are determined from turbulence-generating gird where *m* is the maximum dimensional length of a grid in the grid system.

The RMS value of longitudinal velocity fluctuations, $<u> = \sqrt{[\{\sum_{i=1}^{n}(u_i - U_{av})^2\}/n]}$ where u_i is the instantaneous longitudinal velocity, U_{av} is the average velocity in *X*-direction $=[(\sum_{i=1}^{n}u_i)/n]$ and *n* is the number of grid on the grid-data plane where the grids near the boundary are not taken into account due to viscous effect.

The interactions of shock wave with different strengths of turbulence are observed numerically. It is one of the innovative techniques where three turbulence regions are selected sequentially in a long test section. The decaying phenomena of the turbulence along the centerline of the test section are observed and this technique is applied to perform the interaction of shock wave with different strengths of turbulence numerically. The shock wave is diffracted at the turbulence grids and due to shock wave diffraction; an unsteady flow field is generated in the wake of the turbulence grids. The unsteady flow field consists of many small vortices and these vortices interact each other when moving along the longitudinal direction. The diffracted shock wave, after moving a small distance from the turbulence grids, converges to form again plane, normal shock and at the same time, the unsteady flow field gradually converts to homogeneous, isotropic turbulence due to the motion of vortices and their interactions. At the near region of the turbulence grids, the interaction effects of vortices are high and these effects decrease as increasing the distance from the turbulence grid and for these reasons, the turbulence decaying

phenomena are observed along the longitudinal distance from the turbulence grid. In Fig.4, the turbulence decaying phenomena are observed clearly at three selected turbulence regions along the centerline of the shock tube. The longitudinal turbulence intensity, $\langle u \rangle / U$ are characterized before interaction and after interaction along the centerline for three turbulent regions where U is the flow velocity behind the incident shock wave and it is determined for shock Mach number 2.25 by Rankine–Hugoniot relations.

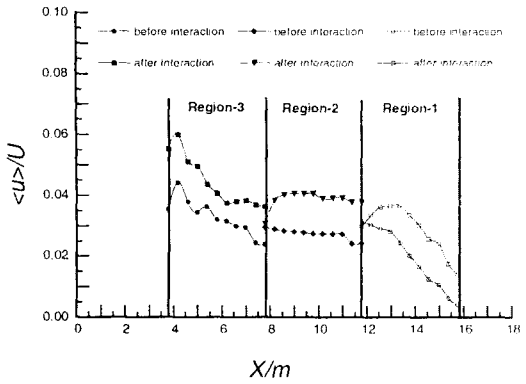

Fig.4: The longitudinal turbulence intensity along the centerline of the turbulent regions before and after the shock wave interaction with different turbulent fields

It is clear in Fig.4 that the strengths of turbulence intensity in three turbulent regions before interaction are different. The outcomes of interaction are the amplification of the longitudinal turbulence intensity and the amplification factor is defined by $\frac{\langle u \rangle_{after\ interaction}}{\langle u \rangle_{before\ interaction}}$. The longitudinal turbulence intensity is amplified by the factor of 1.49 for region-1 and 1.41 for region-2 and 1.36 for region-3. The average amplification factor for these three regions is 1.42 and after considering the three turbulent regions as one region then the overall amplification of turbulence intensity is 1.12. The experimental data of Honkan et al. [9] for shock Mach number 1.354 shows that the amplification factor varies from 1.1 to 1.48. In the present computations, the amplification factor for M_s=2.25 varies from 1.36 to 1.49 in interaction of shock wave with different turbulent fields. The highest amplification of turbulence intensity is 2, which is observed in the experimental data of Briassulis and Andreopoulos [10]. From the results of the LIA data of Lee et al. [11], the maximum amplification of turbulence intensity is close to 2.00 for Mach number range 1.02

to 1.2. From these computations, it is clear that the amplification of longitudinal turbulence intensity in interaction of shock wave with comparatively stronger turbulent field is less than in interaction of shock wave with weak turbulent field. Similarly the amplifications of turbulent kinetic energy (TKE) level are determined for different turbulent regions and it is observed that the amplification of TKE level varies from 1.90-2.10. The maximum amplification factor of TKE level was found 2.00 in the computational results of Rotman [5]. The lateral velocity fluctuations <*v*> in *Y*-direction and the lateral velocity fluctuations <*w*> in *Z*-direction are determined along the centerline of the turbulent regions. It is observed that no substantial amplification of the lateral velocity fluctuations occurs after interaction of shock wave with different turbulent fields. The characteristic behaviors for two components of lateral velocity fluctuations are almost identical which was explained by Barre et al. [12] and confirmed that the two lateral velocity components behave in the same way across the shock.

The average pressure, P_{av}/P_o variations are determined along the longitudinal distance where the average pressure $P_{av}=[(\sum_{i=1}^{n} p_i)/n]$, p_i is the instantaneous pressure for any grid on the grid-data plane and n is the number of grid on the grid-data plane avoiding grids near boundary. P_o is the STD atmospheric pressure. It is observed that no substantial pressure variations occur along the longitudinal distance and slight pressure decreasing are occurred along the far distance in the downstream of the stronger reflected shock wave. It is also observed that no substantial amplification of the pressure fluctuations occurs after interaction.

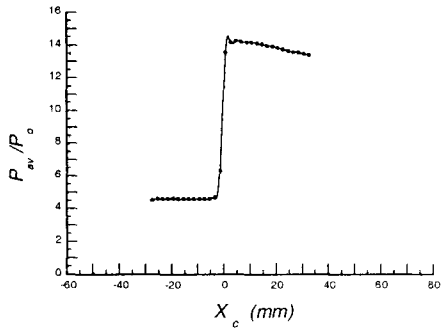

Fig.5: Average pressure profile along the centerline of the turbulent regions (Here $X_c = 0.0$ corresponds to the shock location and $X/m = 9.25$)

Fig.5 shows the average pressure variation across the reflected shock wave when the position of the reflected shock wave is in the turbulent regions. It is shown that the pressure profile across the reflected shock wave obeys the shock reflection theory. Across the reflected shock, there has no average pressure variation occurs in the upstream flow and slight pressure decreasing is observed in the downstream flow due to the stronger reflected shock.

After the interaction of shock wave with different turbulent fields, all the length scales are reduced considerably. There is some disagreement between experimental results and DNS data as far as how the various length scales of turbulence are affected by the interaction with the shock wave. The dissipative-length scale is defined by the expression $k^{3/2}/\varepsilon$ where the turbulent kinetic energy, $k = [(\sum_{i=1}^{n} k_i)/n]$, k_i is the instantaneous turbulent kinetic energy for any grid on the grid-data plane and n is the number of grid on the grid-data plane. Similarly the dissipation rate, $\varepsilon = [(\sum_{i=1}^{n} \varepsilon_i)/n]$ where ε_i is the instantaneous turbulent kinetic energy dissipation rate for any grid on the grid-data plane. The amplification of dissipative-length scale is the ratio of the dissipative-length scale after interaction to the dissipative-length scale before interaction. The different amplifications of dissipative-length scale are determined along the centerline of the turbulent regions due to shock wave interaction with different flow fields and the variations of amplification along the centerline of the turbulent regions is shown in Fig.6.

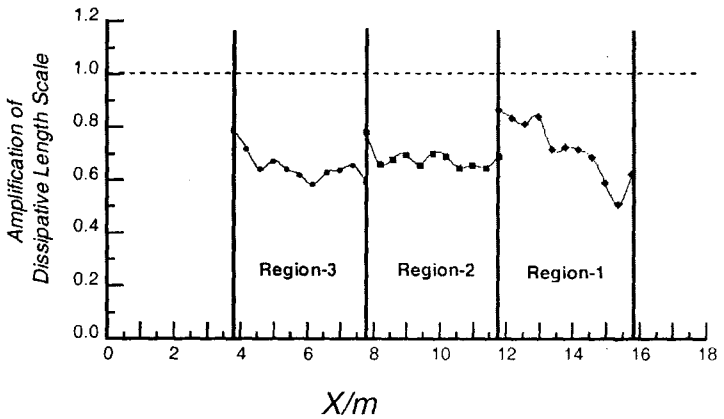

Fig.6: Amplification of dissipative length scale variations along the centerline of the turbulent regions

It is observed that the amplification of dissipative-length scale decreases in all the cases of shock/turbulence interaction. The DNS data of Lee et al. [11] and the DNS data of Hannappel and Friedrich [13] indicate that the velocity length scale and the dissipative-length scale decrease through shock interaction. The dissipative-length scale in the experiment of Honkan and Andreopoulos [14] was found to increase after the interaction. In the present computations, the amplification of dissipative-length scale is decreased after the interaction of shock wave with strong turbulence. Due to stronger compressibility effects, the amplification of dissipative-length scale in shock interaction with stronger turbulence decreases more. The DNS results of Lee et al. [15] have indicated a small increase of dissipative-length scales through weak shock interactions. The length scale is reduced for stronger shock waves while it shows a mild increase for shock waves with shock Mach number less than 1.65. In the present computations, the amplification of dissipative-length scale is decreased after the interaction of shock wave with turbulence. In the case of stronger turbulence, the compressibility level of the flow is high and the shock wave does not compress the scales of turbulence nearly as much and hence the imparted energy tends to remain in the larger scales. In the case of weak turbulence, the shock wave compresses the flow and thus the energy is then moved to the smaller length scales as a result of decreasing the length scale and the outcomes of shock/turbulence interaction are higher.

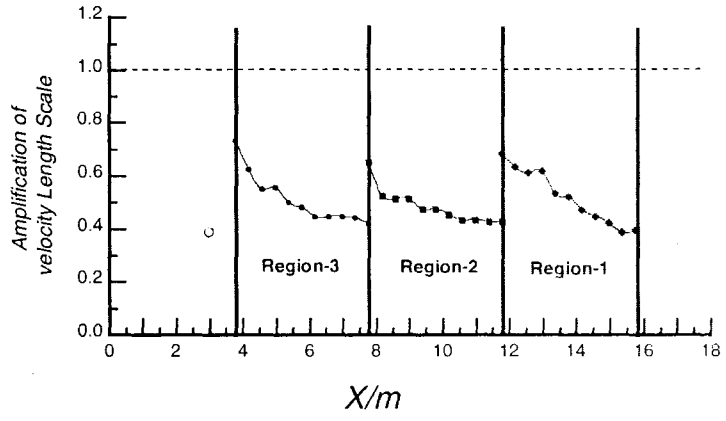

Fig.7: Amplification of velocity length scale variations along the centerline of the turbulent regions

The velocity length scale is defined by the expression $k^{1/2}$. The amplification of velocity length scale is the ratio of the velocity length scale after interaction to the velocity length scale before interaction. The amplifications of velocity length scale are determined along the centerline of the turbulent regions due to shock wave interaction with different flow fields, which is shown in Fig.7. It is observed that the amplification of velocity length scale decreases in interaction of shock wave with different flow fields.

The dissipation rate of turbulent kinetic energy (TKE) is changed depending on the compressibility level of the turbulent field and this value vanishes for incompressible flow. Due to shock wave interaction with the turbulent field of stronger compressibility level, the dissipation rate is decreased more and so more dissipation energy converts to thermal energy or internal energy of the flow. The dissipation rates of TKE are characterized before interaction and after interaction along the centerline of different turbulent regions and the characteristic curves are shown in Fig.8.

It is observed that the dissipation rate is decreased more for turbulent region-3 due to higher compressibility level of the turbulent field in region-3 as compare to other regions and the compressibility effects are higher due to stronger shock/turbulence interaction. For all cases of turbulence strength, the dissipation rate of TKE is decreased after the shock/turbulence interaction and the decreasing of the dissipation rate is higher in interaction of shock wave with comparatively stronger turbulent field.

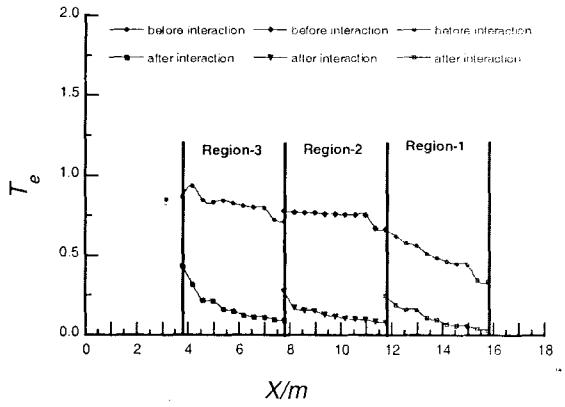

Fig.8: The TKE dissipation rate, T_e ($T_e=10^5\varepsilon$) variations along the centerline of the turbulent regions before and after the shock wave interaction with different turbulent fields

4 Conclusions

A numerical simulation is conducted on the shock wave interaction with different strengths of turbulent fields. The present computational results indicate that the amplification of turbulence intensity and turbulent kinetic energy level depend on turbulence strength as well as the compressibility level of the flow field. Experimentally and numerically many researchers got different values of the amplification of turbulence intensity for weak shock wave interaction with turbulent flow. The amplification for strong shock interaction with strong turbulent field is still questionable matters. The present interaction results provide the important information on strong shock wave interaction with different strengths of turbulent field. After the interaction of strong shock wave with different turbulent fields, all turbulent length scales decrease and this result agrees with other existing computational results. The dissipation rate of turbulence kinetic energy depends on the turbulence strength and the dissipation rate is decreased more in interaction of shock wave with stronger turbulence.

References

[01] Jinnah MA, Takayama K. (2003) Numerical simulation of shock Mach effect on normal shock/homogeneous turbulence interaction. *Computational Methods and Experimental Measurements XI (Proc. of the eleventh international CMEM-2003 conference),* pp. 505-515

[02] Devieve JF, Lacharme JP. 1986, "A shock wave/free turbulence interaction." *Turbulent shear layer/shock wave interaction*, edited by J. Delery, Springer-Verlag, Berlin.

[03] Jacquin L, Blin E, Geffroy P. 1991, "Experiments of free turbulence/shock wave interaction. Proc. Turbulent shear flows, 8, tech Univ, Munich, Ger. pp 1-2-1-1-2-6.

[04] Hesselink L, Sturtevant B. 1988, " Propagation of weak shocks through a random medium." *J. Fluid Mechanics* **196**: 513-553.

[05] Rotman D. 1991, "Shock wave effects on a turbulent flows." *Phys. Fluids* **A, Vol. 3, No. 7:** 1792-806.

[06] Lee S, Lele SK, Moin P. 1991a "Direct numerical simulation and analysis of shock turbulence interaction." *AIAA* paper 91-0523.

[07] Jinnah MA, Takayama K. (2004) Numerical simulation of expansion/compression effect on shock induced turbulent flow. Acceptance on 30th November 2004 for the publication in the journal Comptes rendus de l'Académie des Sciences –Mechanics, INSTITUT DE FRANCE ACADEMIE DES SCIENCES, Paris, France

[08] Sun M, Takayama K. (1999) Conservative smoothing on an adaptive quadrilateral grid, Journal of Computational Physics, 150, pp. 143-180

[09] Honkan, A Watkins CB, Andreopoulos J. (1994) Experimental study of interactions of shock wave with free-stream turbulence, Journal of Fluids Engineering, 116, pp. 763-69.

[10] Briassulis GK, Andreopoulos J. (1996) High resolution measurements of isotropic turbulence interacting with shock waves, Presented at AIAA, Aerospace Sci. Meet., 34th, Reno, NV, 96-004

[11] Lee S, Lele SK, Moin P. (1993) Direct numerical simulation of isotropic turbulence interacting with a weak shock wave, Journal of Fluid Mechanics, 251, pp. 533-62

[12] Barre S, Allem D, Bonnet JP. (1996) Experimental study of a normal shock/homogeneous turbulence interaction, AIAA J, 34, pp. 968-74

[13] Hannappel R, Friedrich R. (1995) Direct numerical simulation of a Mach 2 shock interacting with isotropic turbulence, Appl. Sci. res., 54, pp. 205-21

[14] Honkan A, Andreopoulos J. (1992) Rapid compression of grid-generated turbulence by a moving shock wave, Phys. Fluids, A4, pp. 2562-72

[15] Lee S, Lele SK, Moin P, (1994) Interaction of isotropic turbulence with a strong shock wave, AIAA paper 94-0311 Dept. Mech. Eng., Stanford Univ., CA